

UAV-based Approach to Extract Topographic and As-built Information by Utilising the OBIA Technique

Hairie Ilkham Sibaruddin^{1,2}, Helmi Zulhaidi Mohd Shafri^{1,2,*}, Biswajeet Pradhan³, Nuzul Azam Haron¹

¹Department of Civil Engineering, Faculty of Engineering, Universiti Putra Malaysia (UPM), 43400 Serdang, Selangor, Malaysia

²Geospatial Information Science Research Centre (GISRC), Faculty of Engineering, Universiti Putra Malaysia (UPM), 43400 Serdang, Selangor, Malaysia

³School of Information, Systems & Modelling, Faculty of Engineering and IT, University of Technology Sydney (UTS), Sydney, Australia

*Corresponding author: helmi@upm.edu.my; hzms04@gmail.com

Received August 08, 2018; Revised September 19, 2018; Accepted October 07, 2018

Abstract In this study, the capability of Unmanned Aerial Vehicle (UAV) optical data to provide reliable topographic and as-built information was tested using the eBee Sensefly UAV system. The Object-based Image Analysis (OBIA) technique was used to extract important geospatial information for mapping. The robust Taguchi method was adopted to optimise the segmentation process. Feature space optimisation method was used to obtain the best features for image classification utilising different supervised OBIA classifiers, such as K-nearest neighbour (KNN), normal Bayes (NB), decision tree (DT), random forest (RF) and support vector machine (SVM). Results showed that SVM obtained the highest percentage of overall accuracy, followed by RF, NB, DT and KNN at 97.20%, 95.80%, 93.14%, 86.01% and 77.62%, respectively. The McNemar test was implemented to analyse the significance of the classifier results. The as-built information showed that dimensional accuracy was less than 1 metre compared with ground survey measurement. We conclude that the combination of UAV and OBIA provides a rapid and efficient approach for map updating. This technique could replace the current procedure that utilises piloted aircraft and satellite images for data acquisition and reduce the time for digitising each feature that represents land cover for urban mapping.

Keywords: UAV, land cover, topography map, as-built, OBIA, segmentation

Cite This Article: Hairie Ilkham Sibaruddin, Helmi Zulhaidi Mohd Shafri, Biswajeet Pradhan, and Nuzul Azam Haron, "UAV-based Approach to Extract Topographic and As-Built Information by Utilising the OBIA Technique." *Journal of Geosciences and Geomatics*, vol. 6, no. 3 (2018): 103-123. doi: 10.12691/jgg-6-3-2.

1. Introduction

A topographic map provides important information that represents data on land use and land cover for certain areas. It is a 2D representation of the Earth's 3D landscape. Topographical data also provide an accurate measured plan of a site that encompasses the entire range of various feature information with detailed illustration of man-made and natural features on the ground, such as road, railways, rivers, lakes and buildings. Typically, a topographic map is used as a skeleton for design work before a construction project begins to address the requirements of land survey, urban planning, as-built planning, hazard assessment and disaster risk management.

In the time frame of a mapping survey, a dataset of the topographic map is gathered from platforms, such as space-borne satellites and manned aircraft. Most of the data are acquired by equipment that are too expensive to build and maintain for small-area map updating. In addition, the data are not always within the public domain. The process of acquiring aerial mapping is expensive

given the constraint and requirement to map small areas and using large-format aerial or metric cameras to acquire data is uneconomical and unsuitable [1].

Unmanned Aerial Vehicle (UAV) system operates a powered aerial vehicle without a human operator. UAVs are prominent due to their provision of data with high spatial resolution [2], lightweight sensors and platforms, flexibility of flight planning and deployment and elimination of long dependency [3]. UAVs could also obtain timely imagery of areas that are dangerous or difficult to access by traditional means. This imagery can usually be acquired at a minimum cost or at a cost that is cheaper than that involved in other collection methods [2,3,4]. Current users prefer technologies with low cost but numerous benefits. UAVs are an example of such technologies because they provide highly applicable, immediate and near-real-time data at a resolution that is comparable to that of terrestrial means. UAVs, such as eBee Sensefly are an excellent technology that can provide high capability data for mapping purposes [5].

The features from aerial photo orthomosaic are normally detected and digitised manually from visual interpretation for mapping purposes. However, these methods consume

much time, are tedious and expensive [6]. Automation will provide substantial benefits [4]. The level of automation could range from semi-automatic incorporated with human interaction to completely automated [7]. The potential of acquiring accurate and low-cost UAV data relies on automatic object reconstruction and boundary extraction activities [8].

Pixel-based images analysis are often used to extract low-level features. However, an image is classified according to spectral information, and the pixels in the overlapping region are misclassified; the salt-and-pepper problem thus emerges in the classification result [9] and causes confusion among classes [10]. Meanwhile, Object-based Image Analysis (OBIA) is used to extract high-level features, which constitute shapes in images that are detected regardless of illumination, translation, orientation and scale [7].

Object-based classification for high-spatial-resolution UAV data encounters several challenges despite its highest accuracy among all types of sensors [11]. The scale parameters used for segmentation are much larger than those used for aerial and satellite imagery. The extreme detail on the imagery parses it into many different objects with varying spectral, morphological and proximity characteristics.

Most segmentation processes use trial and error, which is subjective, laborious and time consuming [10]. Hence, a solution to optimise the segmentation process for classification is required. The Taguchi method, which was designed by Dr. Genichi Taguchi, has a simple statistical tool design [12]. This method involves a tabulated design (arrays) system that permits a maximum number of main effects to estimate in an unbiased manner with the lowest number of experimental runs [13]. Several studies had applied this method to optimise the segmentation process in OBIA [10,14,15,16].

Most of the studies have utilised UAV data to produce topographic (DTM, DSM, orthophoto) [17] and land cover maps [11,18,19,20]. However, the data are not fully utilised for as-built plan information. A few studies have highlighted infrastructure information using other sensors,

such as satellite image and aerial laser scanner, for building extraction [21,22,23,24].

Therefore, the first objective of this study is to assess the capability of UAV to provide reliable topographic and as-built data information by utilising the OBIA technique. Specifically, the aim is to determine the most optimal OBIA parameters through segmentation and classification to deliver the required information from UAV data. The segmentation process is important for object classification intended for object-oriented image analysis. This study investigated the effect of parameter tuning with different sample numbers on the overall accuracy of the results to determine the optimal parameter. Machine learning classifiers were used. The second purpose is to extract topographic information, such as land cover features, from UAV data. Lastly, the study aims to extract as-built information, such as infrastructure geometry and dimensions. The geometry from OBIA data was compared from ground truth survey data using a high-accuracy total station equipment.

2. Data and Methods

2.1. Study Area

The study area is situated at the National Land and Survey Institute (INSTUN) in Behrang, Ulu, Tanjung Malim, Perak, Malaysia. The total area of this campus is approximately 200 acres. The area of research interest is limited between latitudes $3^{\circ} 45' 58.3''$ N to $3^{\circ} 46' 2.16''$ N and longitudes $101^{\circ} 30' 34.94''$ E to $101^{\circ} 31' 26.01''$ E, with a total area of 0.3628 km^2 . The study area is surrounded by man-made infrastructures, such as buildings, roads, drainages, sport courts, concrete benches, pavements and parking lots. Natural features, which are dominant, include bare soil, dead grass, grass lands, sand, crops, shrubs and trees. Other features include water bodies, such as swimming pool, lakes, septic tanks and shadows from tall buildings and trees.

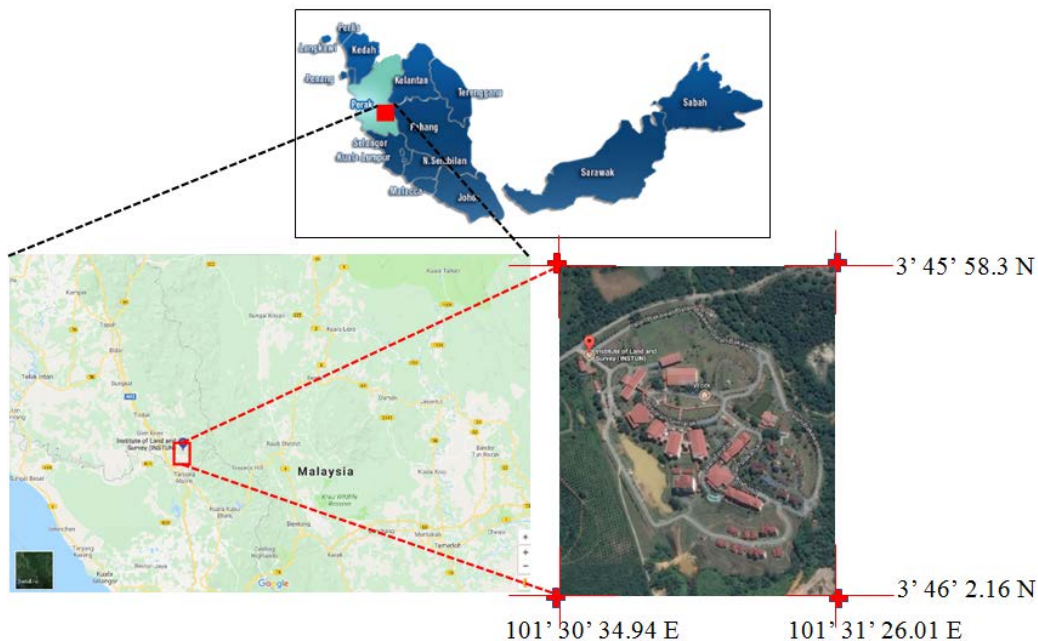


Figure 1. Study area in INSTUN, Perak, Malaysia

2.2. Methodology

The methodology of this research was divided into three phases as shown in Figure 2. The initial phase relied on the acquisition of data from the eBee Sensefly UAV. The orthorectified images were generated using photogrammetric technique. Then, an object-based image analysis, which

involved image segmentation, selection of training and testing samples, image classification, feature selection, tuning parameter setting for each classifier and accuracy assessment, was performed. All related data, such as digital surface model (DSM), digital terrain model (DTM), contour line, image classification output for generating topography map and as-built plan and information, were combined.

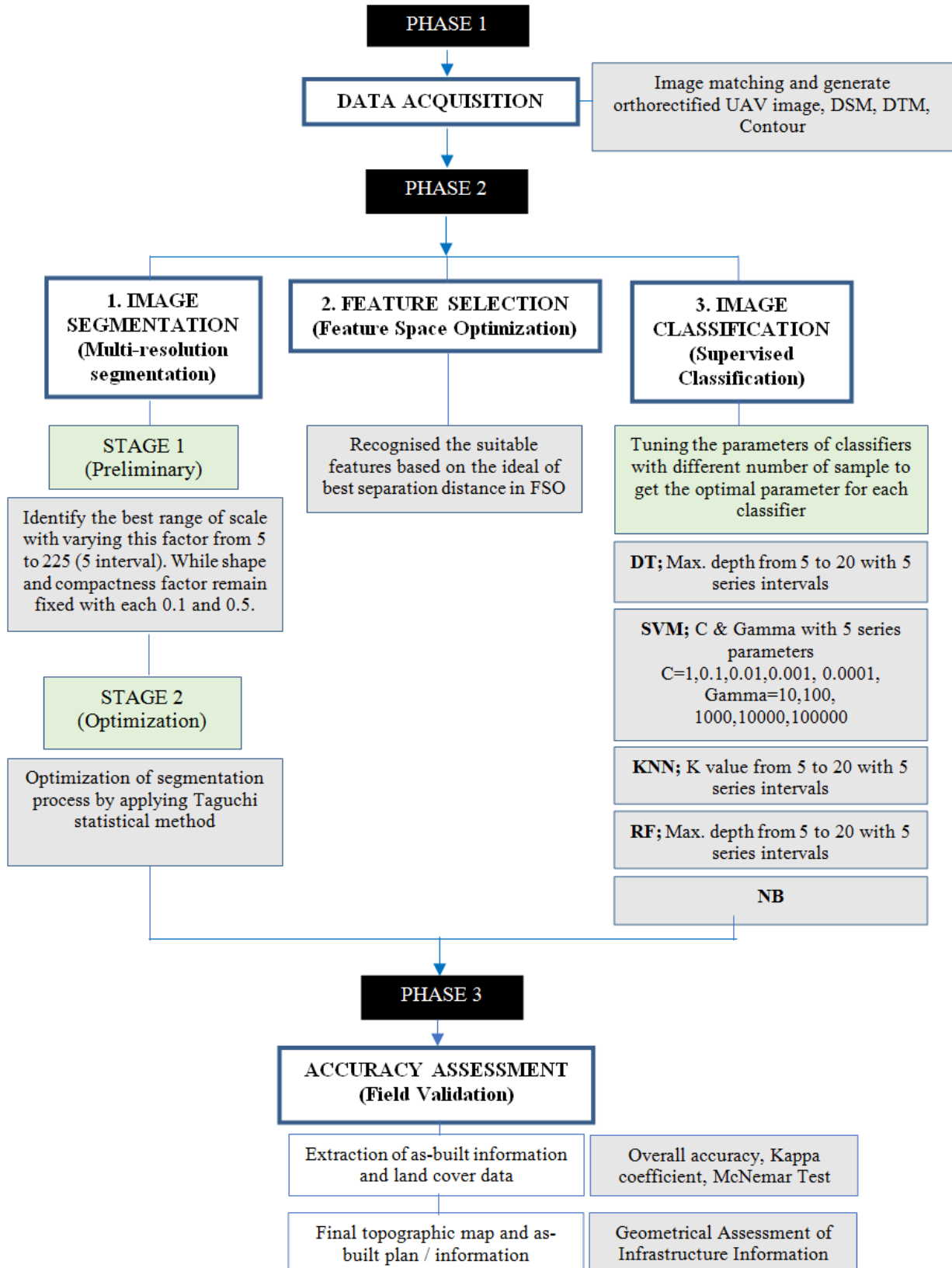


Figure 2. Research methodology flowchart

2.2.1. Phase 1 - Data Acquisition: Pre-processing of UAV Image

The imagery data were obtained on October 18, 2016 using eBee Sensefly UAV. The camera sensor, which is attached on this model, is Canon 16 MP IXUS with a visible colour band (red, green, and blue). During data acquisition, the side lap was 60%, and 80% of the front overlap had been set. The altitude of the UAV was set to 190 m above the ground level. The data were tied with six control points (benchmark and EDM calibration pillars).

The quality check on georeferencing showed that the mean RMS error was 0.025 m. The entire data were set geometrically with the coordinate system WGS84 datum and 47N zone in UTM projection. Raw images were mosaicked to generate an orthorectified image that covered the entire study area by using photogrammetry software Pix4D. The average ground sampling distance (GSD) through this orthorectified image was 5 cm. Seven classes of features were organised and investigated as follows: (1) soil/sand, (2) urban tree, (3) building/roof, (4) impervious surface (other infrastructures), (5) grassland, (6) water body and (7) shadows.

An orthomosaic image with the DSM, DTM and contour line was generated (Figures 3(a-d)) using Pix4D. The image was subjected to automatic radiometric and geometric correction.



Figure 3a. Orthomosaic

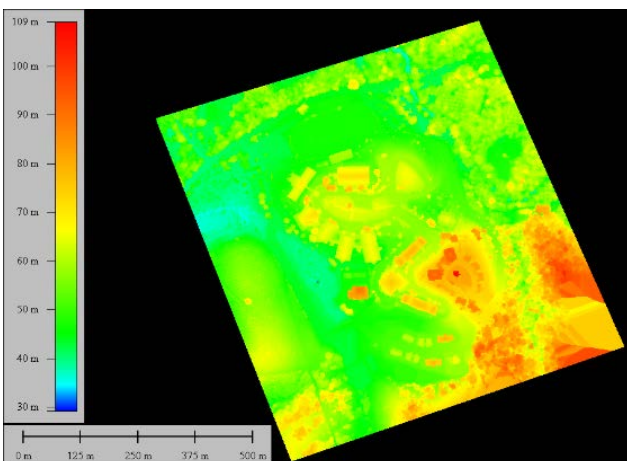


Figure 3b. DTM

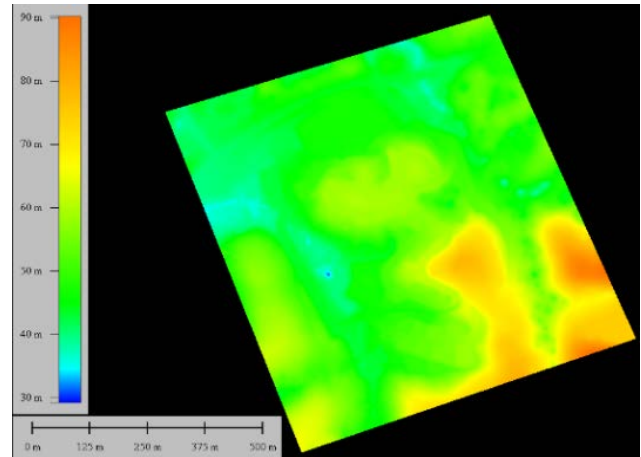


Figure 3c. DSM

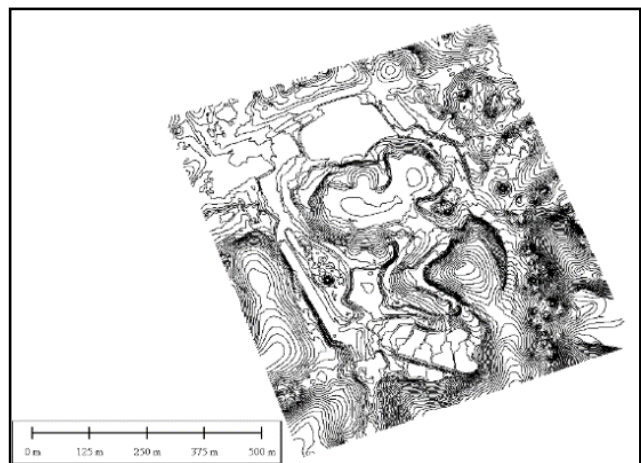


Figure 3d. Contour Line (1m)

2.2.2. Phase 2 - Segmentation and Classification

The initial and most important process during the implementation of the OBIA technique is the segmentation to divide an image into meaningful sections that are correlated to objects in the real world, as shown in the image [25]. Multi-resolution segmentation is a type of bottom-up, region-based segmentation algorithm [26] and is applied using the software e-Cognition version 9.0. Image classification accuracy is promptly controlled with the quality of the segmentation, which is in turn controlled by defined parameters [27]. The three parameters in the multi-resolution segmentation process are as follows: scale, shape and compactness.

The most effective parameter that affects the average image object size is the scale factor [25,28,29]. This factor is controlled by the spatial resolution of the image and features [9,12]. Shape and compactness factors are associated with colour density and smoothness. Then, the amount of spectral information that should be aggregated to build the segments is identified [14]. Initially, to obtain the best range of the scale parameter for image segmentation, a trial and error process was conducted in this work. The selected scale on segmentation was further optimised by applying the Taguchi method.

The segmentation process began with defining the possible range of multi-resolution segmentation parameters to identify the pertinent value of the scale and homogeneity

parameter. The analysis was performed with different scale factors at 5, 25, 50, 75, 100, 125, 150, 175, 200 and 225. Visual interpretation was performed to identify the reliability of the segmented image. The main criterion was that the image object was under-segmented, and the over-segmented image object is eliminated. Previous studies [17,25,30] have consistently emphasised the scale parameter while the other factors remained constant. The shape parameter was set to 0.1, and compactness was set to 0.5 in all 10 preliminary tests to generate meaningful segmented objects. Both parameters used these default values for image segmentation.

The five best results of preliminary segmentation were identified via visual interpretation. The advantages of the Taguchi method include minimising the number of experiments [15] by adopting a fractional factorial design and maintaining a consistent and simple experimental design. This system approach can significantly reduce the total testing time and experimental cost [31]. The Taguchi orthogonal array disperses the parameter equally, and the column depicts independent orthogonal variables to guarantee an impartial comparison of all variables in each level and to examine each parameter separately [32]. The experiment uses an orthogonal array within each pair of columns that corresponds as independent variables. Level combination exists in an equal number of times [13,14,33].

The orthogonal array design by Taguchi is limited to only the combinations of 25 experiments with 3 varying main parameters rather than considering 125 (5x5x5) experimental probabilities. The Taguchi orthogonal array was applied here using Minitab v.17 software. Prior to undertaking the statistical Taguchi optimisation, five levels of the three parameters were defined, as illustrated in the following table.

Table 1. Level for segmentation parameters

PARAMETER	LEVEL				
	1	2	3	4	5
Scale	25	50	75	100	125
Shape	0.1	0.3	0.5	0.7	0.9
compactness	0.1	0.3	0.5	0.7	0.9

Then, the statistical Taguchi method and the spatial objective function were fused in a particular process to optimise the segmentation parameters [33,34]. The idea of combining statistical and spatial (objective function) optimisation methods in a particular process is to model the optimal parameters that guarantee an acceptable quality of segmentation [14]. The objective function is accomplished with the fusion of spatial autocorrelation and variance indices to identify relevant segmentation [35]. Spatial autocorrelation implies the level of distinctiveness between regions (heterogeneity). The variance indicator shows the uniqueness (homogeneity) of the pixels in a single segment [34]. Hence, the condition of good-quality segmentation with the consequences of intra-segment homogeneity and inter-segment heterogeneity is strictly maximised [14].

The first element computed is the intra-segment variance of the regions created by a segmentation algorithm using the equation 1 [34].

Intra-segment variance,

$$v = \frac{\sum_{i=1}^n a_i v_i}{\sum_{i=1}^n a_i} \quad (1)$$

where a_i and v_i refer to area and variance respective to region i , respectively. Intra-segment variance v is a weighted average, where the weights are the areas of each region. The second element assessed is intersegment heterogeneity. The function employs Moran's I autocorrelation index [36]. It quantifies the degree of spatial affiliation as reflected in the data as a unit [34].

Moran's I index is expressed as follows:

$$I = \frac{n \sum_{i=1}^n \sum_{j=1}^n w_{ij} (y_i - \bar{y})(y_j - \bar{y})}{\left(\sum_{i=1}^n (y_i - \bar{y})^2 \right) \left(\sum_{i \neq j} w_{ij} \right)} \quad (2)$$

where n represents the total number of regions and w_{ij} is the spatial weight between objects i and j . y_i is the mean grey value of region R_i , and \bar{y} is the mean grey value of the image (1 for adjacent regions and 0 otherwise). The test was executed, and the corresponding plateau objective of function (POF) was computed for each test based on the combination of parameter level in the orthogonal arrays. The test with the highest result of POF revealed the best performance and was marked as the strength of the quality of optimisation [34]. The objective function (F) was combined with the within-segment variance (v) measure and the between-segment autocorrelation of Moran's I index (I) [34]. It can be expressed as follows:

$$F(v, I) = F(v) + F(I) \quad (3)$$

where $F(v)$ and $F(I)$ are the normalisation functions.

$$F(x) = \frac{X_{\max} - X}{X_{\max} - X_{\min}} \quad (4)$$

Subsequently, the signal-to-noise (SN) ratio was employed to model the optimal segmentation parameters. The three types of SN ratio analysis were applied as follows: (1) lower is better (LB), (2) nominal is the best and (3) higher is better (HB). The aim of this experiment was to optimise the segmentation parameter for image data. Hence, the HB category of the SN ratio was used for modelling. The SN ratio for each experiment was calculated using mean value y_i and variance s_i by determining the effect of each variable. It can be expressed as follows [14]:

$$SN_i = 10 \log 10 \frac{\bar{y}_i^2}{s_i^2} \quad (5)$$

where \bar{y} is the mean and s_i refers to variance as denoted by the equation.

$$\bar{y}_i = \frac{1}{N_i} \sum_{u=1}^{N_i} y_{i,u} \quad (6)$$

$$s_i^2 = \frac{1}{N_i - 1} \sum_{u=1}^{N_i} (y_{i,u} - \bar{y}_i)^2 \quad (7)$$

In Equations (6) and (7), i is the number of experiments, u is the trial number and N_i is the number of trials in experiment i . The average SN ratio was employed to evaluate the result of each experiment. A high SN ratio denotes the optimal parameter segmentation based on Equation (8). The average of the SN value for each level and factor was derived. Then, the result was exported as a table and a graph.

$$SN_i = -\log_{10} \left[\frac{1}{N_i} \sum_{u=1}^{N_i} \frac{1}{y_u^2} \right] \quad (8)$$

Seven classification classes were identified and are illustrated in Table 2.

The training and testing samples were selected randomly based on experience from ground truth assessment data on the study area. The sample was divided into five parts to check the classification accuracy and to examine the influences of classifiers on the sample size; 70% of the sample was used for training and 30% for testing. Each training and testing sample was selected differently to ensure that no repeated sample was selected for accuracy assessment.

An assessment using different numbers of samples for training and testing was also conducted by tuning the parameter for each classifier while excluding NB to obtain the relationship with the various parameters being set for optimising the classification result. The different numbers of samples for each class were selected randomly due to different areas for each class. The soil/sand class with the highest number of object classes was selected, followed by urban tree, building/roof, grassland, impervious surface, water and shadow, as shown in Table 3.

After selecting the training sample, spectral and spatial features were required to classify the image. Feature space optimisation (FSO) tools, which are available in e-Cognition software, were used for feature selection. More than hundreds of features are available for classification. A total of 41 features were selected for FSO to identify the appropriate features for further classification [18]. The object features were used and processed for further analysis with different training and testing sizes. The features were divided into shape, texture and spectral properties. The values of best separation distance for samples 1, 2, 3, 4 and 5 were 3.975, 2.545, 2.166, 2.063 and 1.882, respectively. Sample 1 with 100 training data samples had the highest separation distance compared with the other data samples.

Five machine learning classification algorithms that are K-nearest neighbour (KNN), normal Bayes (NB), decision tree (DT), random forest (RF) and support vector machine (SVM) were used and tested thoroughly to evaluate their performance under varying conditions and to optimise their applicability in terms of the OBIA technique. To optimise the parameter for each classifier, several tests were performed by tuning the parameter for each classifier, except for NB with one available parameter for adjustment. The sensitivity of each classifier was examined using the selected training and testing samples by referring to the results of the accuracy assessment and by varying their respective parameters.

NB is a simple technique for constructing classifiers by applying the Bayes theorem (Bayesian statistics) [37]. It is not a single algorithm for training classifiers; it is a family of algorithms based on a common principle. The NB classifier assumes that the value of a particular feature is independent. The data distribution function with one component per class is assumed to be a Gaussian mixture. The algorithm estimates the mean vectors and covariance matrices of the selected features for each class for classification. The advantage of the NB classifier is that it does not require any parameter to tune, which could be subjective and time consuming.

The KNN algorithm is a method for classifying objects based on closest training examples in the feature space. KNN is a non-parameter algorithm for instance-based learning or lazy learning [38]. An object is classified by referring to the class attributes of its KNN parameters. Therefore, K is the key tuning parameter in this classifier, and it is largely determined the performance of the KNN classifier [37]. In this study, the K values varied from 5 to 20 with 5 intervals each to identify the optimal K value for all training sample sets.

DT learning is a method used in data mining, in which a series of decisions are made to segment data into homogeneous subgroups. The aim is to create a model that predicts the value of a target variable based on several input variables. This process is repeated on each derived subset in a recursive manner (recursive partitioning). The recursion is completed when the subset at a node has the same value as the target variable or when splitting no longer adds value to the predictions. The purpose of analyses via tree-building algorithms is to determine a set of if-then logical (split) conditions [38]. During this study, we tested the value of maximum depth from 1 to 20 for all five training samples. The other parameters, such as cross validation folds and min sample count, were set to 10 (default). Other factors remained constant.

Table 2. Types of image classification

NO.	NAME OF CLASSES	DESCRIPTION
1	Soil/Sand	All bare sand/soil and/or very/dead grasslands
2	Urban Tree	All type of crop, shrub, bush, oil palm tree species canopies
3	Building/Roof	All different size building or roofs with different material cover
4	Grass Land	All type of grass lands
5	Other Infrastructures (Impervious Surface)	All impervious surface areas e.g. road, park lots, pavement, tennis court, volleyball court, bench, jetty, drainage, sump
6	Water	All different types of water bodies (lake, swimming pool, septic tank)
7	Shadow	All shadows from building, tree (light and dark shadow)

RF, also referred to as random tree, is an ensemble of decision trees [37]. The random tree classifier is more of a framework than a specific model. It uses an input feature vector and classifies it with every tree in the forest.

It results in a class label of the training sample in the terminal node, where it ends [38]. The value of the maximum depth was set from 1 to 20 for all five training samples in this study. The other parameters, such as cross validation folds and min sample count, were set to 10 (default).

SVM constructs a hyperplane or a set of hyperplanes in an infinite dimensional space, which can be used for

classification and regression analysis. The most frequently used types of kernel functions or SVM algorithms are linear, polynomial and radial basis functions (RBF) and sigmoid kernels [37]. In this study, the RBF kernel, which is the most frequently used and has been proven superior to other kernels, was adopted. The RBF kernel has two important tuning parameters: cost (C) and Gamma. The optimal values of C and Gamma are often estimated with the exhausted search method. We systematically tested five different values of C and Gamma to examine the effect of these two key parameters on the performance of SVM within the object-based approach.

Table 3. Tabulation of training and testing sample objects for each class

SAMPLE	NUMBER OF OBJECTS FOR EACH CLASS														TOTAL	
	SOIL / SAND		URBAN TREE		BUILDING / ROOF		GRASSLAND		OTHER INFRASTRUCTURE S (IMPERVIOUS SURFACE)		WATER		SHADOW			
	TRAINING	TESTING	TRAINING	TESTING	TRAINING	TESTING	TRAINING	TESTING	TRAINING	TESTING	TRAINING	TESTING	TRAINING	TESTING	TRAINING	TESTING
SAMPLE 1	27	12	23	10	17	7	13	6	10	4	7	3	3	1	100	43
SAMPLE 2	53	23	47	20	33	14	27	11	20	9	13	6	7	3	200	86
SAMPLE 3	80	35	70	30	50	21	40	17	30	13	20	9	10	4	300	129
SAMPLE 4	107	46	93	39	67	29	53	23	40	17	27	11	13	6	400	171
SAMPLE 5	133	57	117	50	83	36	67	29	50	21	33	14	17	7	500	214

2.2.3. Phase 3 - Accuracy Assessment

Object-based accuracy assessment is a measure of a statistical output to confirm the quality of classification results. The method that is most often used to assess accuracy is based on an error matrix. It utilises appropriate accuracy measures to compare different classification techniques [39,40]. An error matrix is a cross tabulation of the classes of the classified imagery and reference data. It offers a form of site-specific assessment of the correspondence or accuracy degree of the classified image and the objects in the site [40]. In general, overall accuracy, producer accuracy, user accuracy and kappa coefficient are computed from an error matrix [41].

McNemar test was performed to examine the role of each classifier. This test identifies a change in the proportion of the paired data to determine whether the statistical differences in classification accuracies are quantitatively significant [42]. This statistical test uses a non-parametric approach based on the statistics of a 2 × 2 matrix [43]. The assessment relies on chi square (x²) distribution and indicates the statistical differences by measuring the z score under the null hypothesis that classification is different. A z score > 1.645 shows the confidence level at 95% quantitative significance (p-value of 0.05) with one degree of freedom [43]. The McNemar test represents the statistical difference by measuring a z score under the null hypothesis that the classifications are different. The formula is expressed as follows:

$$x^2 = \frac{(f_{12} - f_{21})^2}{f_{12} + f_{21}} \tag{9}$$

where *f*₁₂ and *f*₂₁ indicate the number of ground truth data samples accurately classified in a set of classification but inaccurately classified in another classifier. These values are extracted from the data obtained from the classified image performed by classifiers 1 and 2 [44].

Three classes of land cover, including building/roof and impervious surface (drainage, road), were selected for as-built geometrical assessment. Ground truth data were collected using survey equipment, such as total station for the area. The area of assessment was selected as the area of staff quarters in INSTUN.

3. Results and Discussions

3.1. Results of Preliminary Segmentation

Figure 4(a) to Figure 4(i) show the result of the preliminary segmentation using the trial and error method. The result shows that the scale parameters of 25, 50, 75, 100 and 125 results in relevant and acceptable segmentation against other under-segmented objects for the seven selected classes. The result was selected based on the

criterion of segmented images, that is, an acceptable under-segmented area with a minimum number of over-segmented and under-segmented objects. Therefore, the

five best segmentation results with different scale parameters were selected for further optimisation segmentation using the Taguchi method.

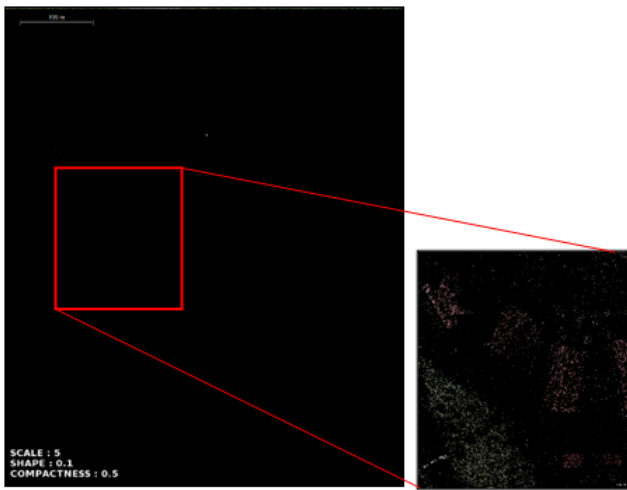


Figure 4a. (scale: 5)



Figure 4d. (scale: 75)



Figure 4b. (scale: 25)



Figure 4e. (scale: 125)



Figure 4c. (scale: 50)



Figure 4f. (scale: 125)

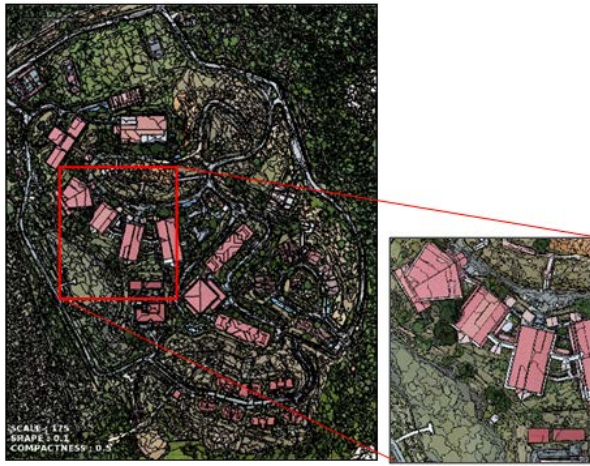


Figure 4g. (scale: 150)

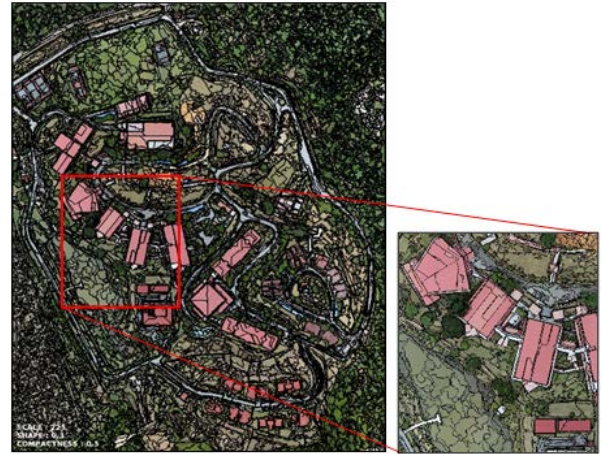


Figure 4i. (scale: 200)



Figure 4h. (scale: 175)



Figure 4j. (scale: 225)

Table 4. Calculation of the plateau of function

TEST	SCALE	SHAPE	COMPACTNESS	NO. OF OBJECTS	AREA x VARIANCE	INTRASEGMENT VARIANCE, V	MORAN INDEX, I	NORMALISED INTRASEGMENT VARIANCE	NORMALISED MORAN INDEX	PLATEAU OF FUNCTION (POF)
T1	25	0.1	0.1	292,213	284130067.530	2.249	0.616	1.000	0.474	1.474
T2	25	0.3	0.3	287,426	298346842.852	2.361	0.648	0.943	0.392	1.335
T3	25	0.5	0.5	260,712	323533915.878	2.561	0.695	0.841	0.271	1.112
T4	25	0.7	0.7	234,312	357738466.997	2.831	0.717	0.703	0.216	0.920
T5	25	0.9	0.9	218,477	402621039.637	3.187	0.801	0.522	0.000	0.522
T6	50	0.1	0.3	87,752	328136522.871	2.597	0.537	0.823	0.678	1.500
T7	50	0.3	0.5	85,306	348098896.005	2.755	0.590	0.742	0.5411	1.283
T8	50	0.5	0.7	77,416	378344200.146	2.994	0.595	0.620	0.528	1.148
T9	50	0.7	0.9	70,892	414181950.923	3.278	0.627	0.476	0.447	0.923
T10	50	0.9	0.1	34,039	441788694.166	3.497	0.660	0.364	0.362	0.726
T11	75	0.1	0.5	43,599	355906725.097	2.817	0.492	0.711	0.791	1.502
T12	75	0.3	0.7	41,928	381758887.938	3.021	0.539	0.606	0.673	1.279
T13	75	0.5	0.9	38,796	414811875.785	3.283	0.540	0.473	0.671	1.143
T14	75	0.7	0.1	25,934	419955643.806	3.324	0.552	0.452	0.639	1.091
T15	75	0.9	0.3	17,682	481076393.238	3.807	0.572	0.206	0.588	0.794
T16	100	0.1	0.7	26,753	377440063.122	2.987	0.447	0.624	0.907	1.530
T17	100	0.3	0.9	25,778	409356725.481	3.240	0.467	0.495	0.857	1.352
T18	100	0.5	0.1	20,111	412286184.941	3.263	0.513	0.483	0.737	1.221
T19	100	0.7	0.3	15,637	447083102.610	3.538	0.493	0.343	0.790	1.133
T20	100	0.9	0.5	11,949	509986184.541	4.036	0.527	0.089	0.702	0.791
T21	125	0.1	0.9	18,389	396797572.505	3.140	0.411	0.546	1.000	1.546
T22	125	0.3	0.1	16,072	407003727.068	3.221	0.433	0.505	0.943	1.447
T23	125	0.5	0.3	13,728	432107332.699	3.420	0.442	0.403	0.920	1.324
T24	125	0.7	0.5	10,878	470710222.563	3.725	0.430	0.248	0.951	1.199
T25	125	0.9	0.7	9,029	532115563.727	4.211	0.493	0.000	0.791	0.791

3.2. Results of Optimised Segmentation Using the Taguchi Method

Table 4 shows the result of each test in which several equations were evaluated to identify the optimised parameter for image segmentation. Refer to Table 4, it shows that the highest score for POF was the combination of scale, shape and compactness in levels 5, 1 and 5, respectively, with a score of 1.546. Further interpretation of the table reveals that a POF value with the highest POF in a pattern is in agreement with the analysed SN ratio result [14]. The hybrid strategy slightly carried the orthogonal vectors and POF to calculate the SN ratios.

Figures 5(a) and 5(b) present the main effect plots of the means and SN ratios for multi-resolution segmentation. The response table for mean and SN ratio obtained from the analysis of the Taguchi method is presented in Tables 5a and 5b. The result shows that the optimum combination yielded the highest value of SN ratios and means with the associate of level 5 (125) for scale, level 1 (0.1) for shape and level 2 (0.3) for compactness.

Table 5a. Response table for mean

LEVEL	SCALE	SHAPE	COMPACTNESS
1	1.0726	1.5105	1.1919
2	1.1162	1.3393	1.2171
3	1.162	1.1896	1.1774
4	1.2054	1.053	1.1337
5	1.2613	0.7249	1.0973
Delta	0.1887	0.7856	0.1198
Rank	2	1	3

Table 5b. Response table for SN ratio (larger is better)

LEVEL	SCALE	SHAPE	COMPACTNESS
1	0.08617	3.58125	1.25871
2	0.6831	2.52891	1.50894
3	1.118	1.49106	1.23246
4	1.41904	0.39794	0.85407
5	1.79329	-2.89954	0.24543
Delta	1.70712	6.48079	1.26351
Rank	2	1	3

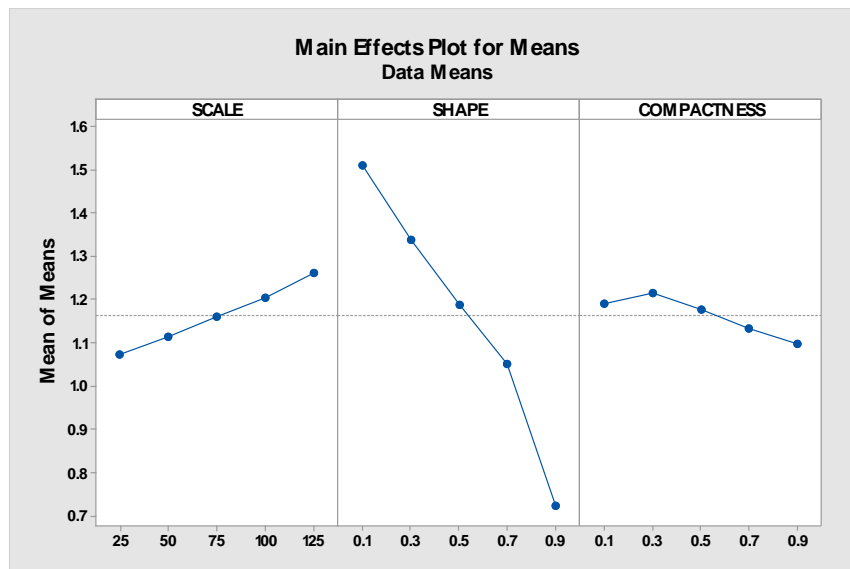


Figure 5a. Main effect plot (data means)

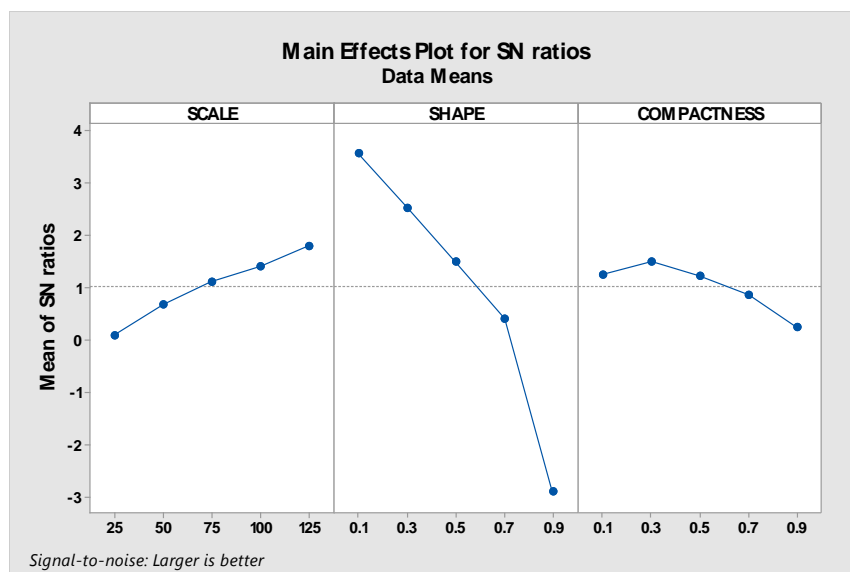


Figure 5b. Main effect plot (SN ratio)



Figure 6a. Building & bare soil

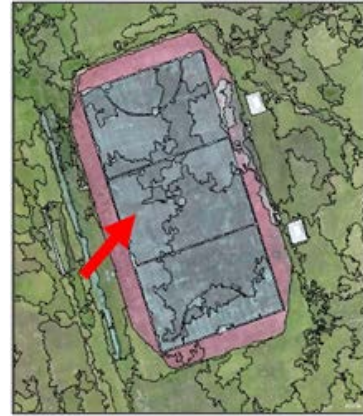


Figure 6e. Volleyball court (Impervious Surface)



Figure 6b. Road



Figure 6f. Shadow



Figure 6c. Water bodies & grassland

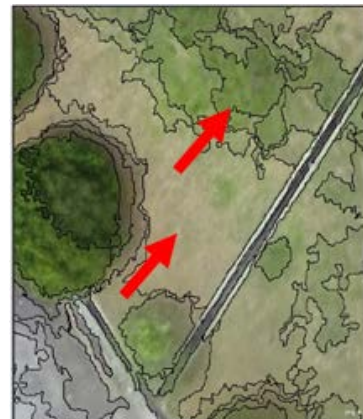


Figure 6g. Bare soil & grassland



Figure 6d. Urban tree



Figure 6h. Water bodies & Jetty (Impervious Surface)

Visual judgement confirmed that the optimised segmentation parameters yielded the utmost results after applying the Taguchi method, as shown in Figure 6(a) to Figure 6(h). Therefore, the merging of the statistical and spatial optimisation processes creates intrinsic sensitivity to the image pixels and their spatial relationship. The strength of these properties is utilised to obtain the desired quality.

3.3. Results of Image Classification

3.3.1. Effects of Parameter Tuning of the Classifiers

The tuning parameter of the classifier tremendously influenced the classification accuracy. The SVM classifier showed high impact and sensitivity to the tuning parameter, with a variation of up to 60% for each data sample from the result of minimum to maximum overall accuracy. The variation of KNN showed decreasing accuracy with increasing K parameter for all data samples; it is different from the RF classifier, in which the turning point is at the maximum depth parameter of 15. When the depth was more than 15, the overall accuracy suddenly decreased for all data samples. For DT, the trends showed increasing overall accuracy with the increase in the maximum depth parameter for all data samples. However, most of the data samples provided the highest result as the parameter reached 20.

Therefore, the optimal parameter setting for SVM varied with the data sample size. The optimum values for

C and Gamma were 100,000 and 0.001 for samples 2 and 5, respectively, and the result obtained was better than that of the other sample combinations, which affected the accuracies of the SVM classification. Most of the data showed that regardless of the value of C, the overall accuracy decreases when Gamma increases to 0.001; the effect is a decrease in OA. The ranges of C and Gamma factors in all samples indicate that up to 90% accuracy can be obtained with a Gamma value of 0.1.

Moreover, with a small size of the data sample, a Gamma parameter of up to 0.0001 may negatively affect accuracy, which can only reach up to 50% of OA. On the contrary, with a sample size of up to 300, OA may consistently be within the minimum of 75% up to 97% with increasing sample data. Thus, the effect of tuning parameter is caused by OA, given that a small sample size (e.g. sample 1 with C and Gamma at 10 and 0.1) results in OA of up to 92%. The performance of NB, KNN, RF, DT and SVM classifiers with different sample sizes is shown in Figure 7 to Figure 8 and Table 6 to Table 11.

Table 6. Overall accuracy of NB with the increment in sample data

NB CLASSIFIER	OA	KC
SAMPLE 1	81.12	0.760
SAMPLE 2	90.90	0.887
SAMPLE 3	91.60	0.896
SAMPLE 4	92.64	0.909
SAMPLE 5	93.14	0.915

Table 7. Variation of parameter K with proportion to the size of sample data

KNN CLASSIFIER	K=5		K=10		K=15		K=20		K=25	
	OA	KC	OA	KC	OA	KC	OA	KC	OA	KC
SAMPLE 1	77.62	0.721	69.93	0.623	66.43	0.571	65.03	0.551	61.54	0.506
SAMPLE 2	73.08	0.661	69.23	0.615	65.73	0.562	64.34	0.542	62.24	0.515
SAMPLE 3	72.49	0.662	66.90	0.583	66.20	0.573	63.17	0.536	61.07	0.506
SAMPLE 4	73.38	0.669	68.13	0.596	64.80	0.551	64.27	0.545	62.87	0.524
SAMPLE 5	71.99	0.653	67.79	0.597	65.69	0.564	64.29	0.548	63.45	0.536

Table 8. Variation of depth parameter with proportion to the size of sample data

RF CLASSIFIER	DEPTH=5		DEPTH=10		DEPTH=15		DEPTH=20		DEPTH=25	
	OA	KC	OA	KC	OA	KC	OA	KC	OA	KC
SAMPLE 1	93.01	0.914	95.10	0.940	95.21	0.942	95.10	0.940	95.10	0.940
SAMPLE 2	76.84	0.717	93.36	0.918	95.80	0.948	95.45	0.944	93.71	0.923
SAMPLE 3	76.22	0.711	89.74	0.874	92.07	0.903	91.38	0.894	91.38	0.894
SAMPLE 4	76.53	0.713	88.79	0.863	92.29	0.906	91.24	0.893	91.24	0.893
SAMPLE 5	74.79	0.694	87.39	0.846	89.08	0.867	88.80	0.863	89.36	0.870

Table 9. Variation of parameter depth with proportion to the size of sample data

DT CLASSIFIER	DEPTH=5		DEPTH=10		DEPTH=15		DEPTH=20		DEPTH=25	
	OA	KC	OA	KC	OA	KC	OA	KC	OA	KC
SAMPLE 1	81.82	0.776	85.31	0.821	85.31	0.821	86.01	0.830	85.31	0.821
SAMPLE 2	73.08	0.670	83.92	0.805	83.22	0.796	84.27	0.809	83.22	0.796
SAMPLE 3	68.53	0.618	75.99	0.711	75.99	0.711	76.13	0.717	75.76	0.709
SAMPLE 4	70.75	0.644	83.19	0.796	82.66	0.790	82.66	0.790	82.66	0.790
SAMPLE 5	71.57	0.646	77.87	0.731	79.27	0.746	79.13	0.745	79.31	0.749

Table 10. Variation of the combination of parameter C and Gamma with proportion to the size of sample data

SVM CLASSIFIER		SAMPLE 1		SAMPLE 2		SAMPLE 3		SAMPLE 4		SAMPLE 5	
C	GAMMA	OA	KC	OA	KC	OA	KC	OA	KC	OA	KC
10	1	78.32	0.724	79.02	0.735	78.79	0.731	78.46	0.727	77.17	0.714
	0.1	92.31	0.905	89.51	0.870	87.88	0.850	88.97	0.863	77.17	0.714
	0.01	81.12	0.763	74.83	0.681	75.99	0.698	76.01	0.698	76.19	0.702
	0.001	54.55	0.390	51.75	0.354	55.01	0.403	56.57	0.424	55.18	0.405
	0.0001	27.27	0.002	26.57	0.001	26.81	0.001	32.22	0.077	34.31	0.108
100	1	78.32	0.724	79.02	0.735	79.02	0.734	78.46	0.727	78.71	0.730
	0.1	93.71	0.922	92.31	0.905	92.77	0.911	93.17	0.916	93.13	0.916
	0.01	90.91	0.888	89.16	0.866	88.34	0.856	90.89	0.887	92.58	0.908
	0.001	83.22	0.790	75.17	0.686	75.52	0.692	76.88	0.710	77.73	0.722
	0.0001	53.15	0.371	51.75	0.354	55.71	0.413	56.57	0.425	55.00	0.402
1000	1	78.32	0.724	79.02	0.735	79.02	0.734	78.46	0.727	78.71	0.730
	0.1	93.71	0.922	92.31	0.905	93.01	0.914	92.99	0.913	93.00	0.914
	0.01	93.01	0.914	95.10	0.940	93.47	0.920	96.15	0.953	95.94	0.950
	0.001	90.91	0.888	89.86	0.875	90.21	0.879	90.01	0.876	90.76	0.886
	0.0001	82.52	0.781	76.57	0.704	77.16	0.714	76.36	0.703	77.17	0.714
10000	1	78.32	0.724	79.02	0.735	79.02	0.734	78.46	0.727	78.71	0.730
	0.1	93.82	0.931	92.66	0.910	93.01	0.914	92.99	0.913	93.28	0.917
	0.01	93.01	0.914	94.76	0.935	94.41	0.931	96.82	0.958	96.78	0.960
	0.001	92.31	0.905	95.10	0.940	95.80	0.948	95.80	0.948	96.80	0.961
	0.0001	90.91	0.888	88.11	0.853	88.58	0.859	88.62	0.859	89.64	0.872
100000	1	78.32	0.724	79.02	0.735	79.02	0.734	78.46	0.727	78.71	0.730
	0.1	93.71	0.922	92.66	0.910	93.01	0.914	92.99	0.913	93.00	0.914
	0.01	93.01	0.914	95.10	0.940	94.64	0.934	96.15	0.953	96.50	0.957
	0.001	92.31	0.905	96.15	0.953	95.57	0.946	96.15	0.953	97.20	0.966
	0.0001	92.31	0.905	95.45	0.944	95.10	0.940	93.35	0.918	94.82	0.936

3.3.2. Effects of Varying the Number of Selected Samples

The result of the analysis showed that SVM obtained the highest accuracy among the five classifiers in terms of C and Gamma. The minimum result for the overall accuracy and kappa coefficient of SVM for all samples was 93.82% and 0.931, respectively, with the total average of five samples at 95.96% and 0.951. In addition, the overall accuracy of SVM was maintained with an accuracy of more than 90% each. The minimum accuracy of the SVM classifier was better than the highest overall accuracy and kappa coefficient for NB (93.14% and 0.915), DT (86.01% and 0.830) and KNN (77.62% and 0.721). Sample 2 of RF showed the highest overall accuracy and kappa coefficient of 95.80% and 0.948, respectively. Sample 5 of SVM obtained the highest result. The result is contrary to that of Sample 5 of RF, which obtained the lowest overall accuracy and kappa coefficient with the maximum size of sample data. The overall accuracy for NB was consistent in Samples 2 to 5, with an accuracy of more than 90% each. However, with a small number of training and testing data samples, the accuracy decreased to 81.12%. The average accuracy and kappa coefficient of the DT classifier were 81.77% and 0.780, respectively, and Sample 1 obtained the best result. Graphs in Figure 7 and Figure 8 show that KNN obtained the lowest accuracy and kappa values for all data sample sizes compared with the other classifiers.

The size of training and testing data affected the classification accuracy of certain classifiers, such as NB and DT, compared with RF and KNN, which are less sensitive to the increase in sample data. SVM and RF obtained a consistent overall accuracy with the most outstanding result (more than 90%) compared with the other classifiers. The KNN classifier obtained the highest score of 77.62% and 0.721 for accuracy and kappa values, respectively. Hence, increasing the number of data samples did not affect the increase in the overall accuracy of classification.

The result shows that the variation of the size of training samples from 100 to 500 (sample 1 to 5) increased the accuracy of NB and SVM by 12.02% and 3.38%, respectively. On the contrary, the accuracy of DT, RF and KNN decreased to 6.74%, 5.85% and 5.63%, respectively. The NB classifier was the most sensitive to the variation of sample size because the parametric classifier consumes the training samples to estimate the parameter value for data allocation. Hence, with the increasing number of training samples, a highly accurate parameter estimation can be achieved. SVM is the least sensitive to sample sizes because it requires support vectors rather than using all training samples to create a separating hyperplane. Table 11 shows that the classification accuracy of the three classifiers shifted and became inconsistent when Sample 3 with more than 300 samples was selected with a variation of DT (-8.74%), RF (-3.73%) and KNN (-0.59%). This result revealed that

Sample 3 is the turning point among these classifiers. The additional sample size disrupted the accuracy.

Table 11. The best accuracy for each classifier with the variation of the size of sample data

CLASSIFIER / SAMPLE	NB		KNN		RF		DT		SVM	
	OA	KC	OA	KC	OA	KC	OA	KC	OA	KC
SAMPLE 1	81.12	0.760	77.62	0.721	95.21	0.942	86.01	0.830	93.82	0.931
SAMPLE 2	90.90	0.887	73.08	0.661	95.80	0.948	84.27	0.809	96.15	0.953
SAMPLE 3	91.60	0.896	72.49	0.662	92.07	0.903	76.13	0.717	95.80	0.948
SAMPLE 4	92.64	0.909	73.38	0.669	92.29	0.906	83.19	0.796	96.82	0.958
SAMPLE 5	93.14	0.915	71.99	0.653	89.36	0.870	79.27	0.746	97.20	0.966
AVERAGE	89.88	0.873	73.71	0.673	92.95	0.914	81.77	0.780	95.96	0.951

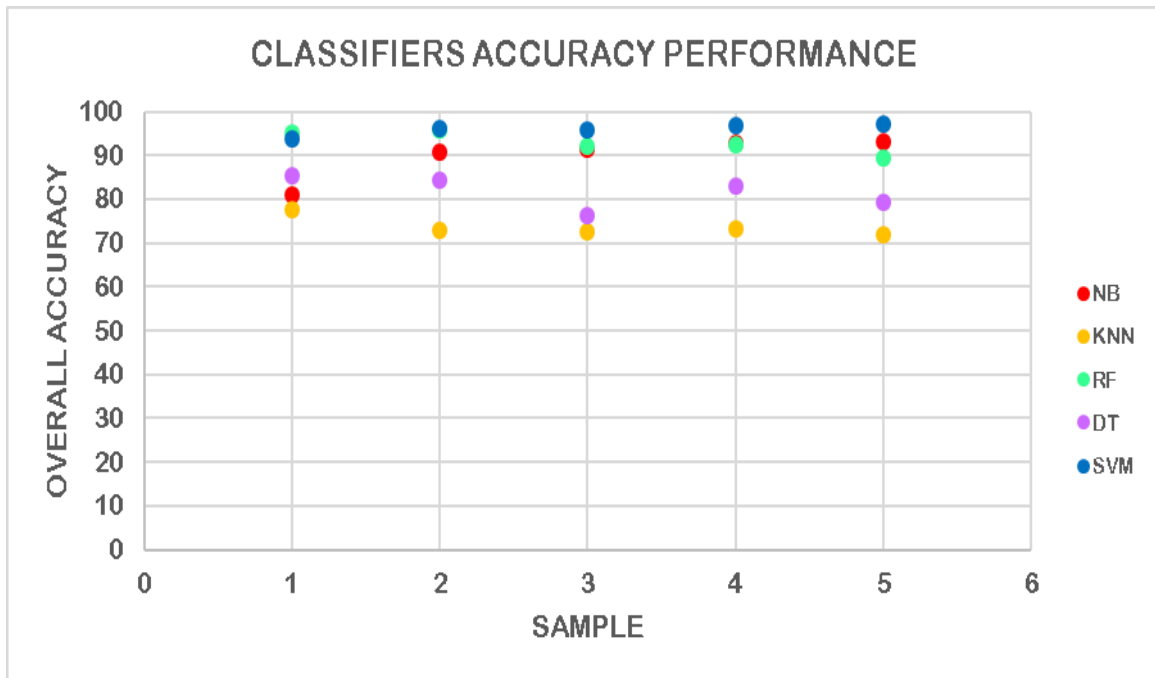


Figure 7. Result of overall accuracies for the best of the five classifiers with increasing sample size

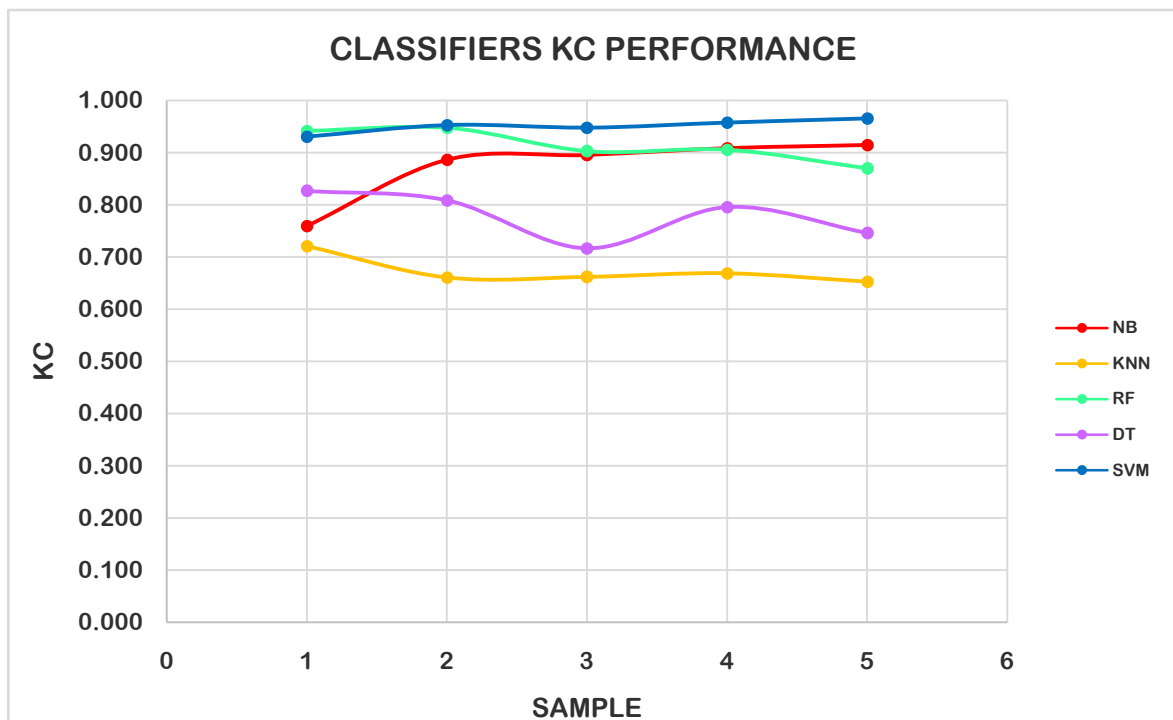


Figure 8. Kappa coefficient (KIA) of the five classifiers with increasing sample size



Figure 9a. Orthomosaic

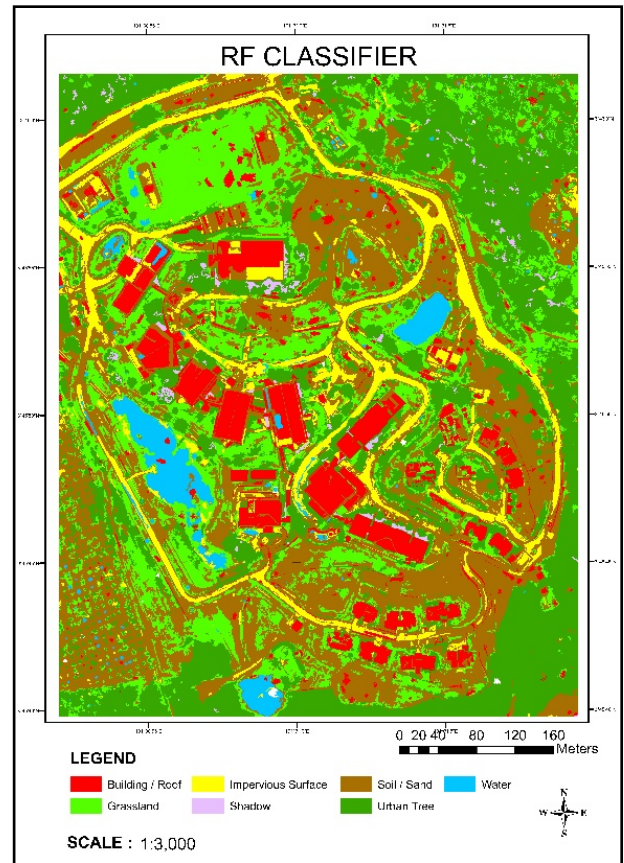


Figure 9c. RF classification

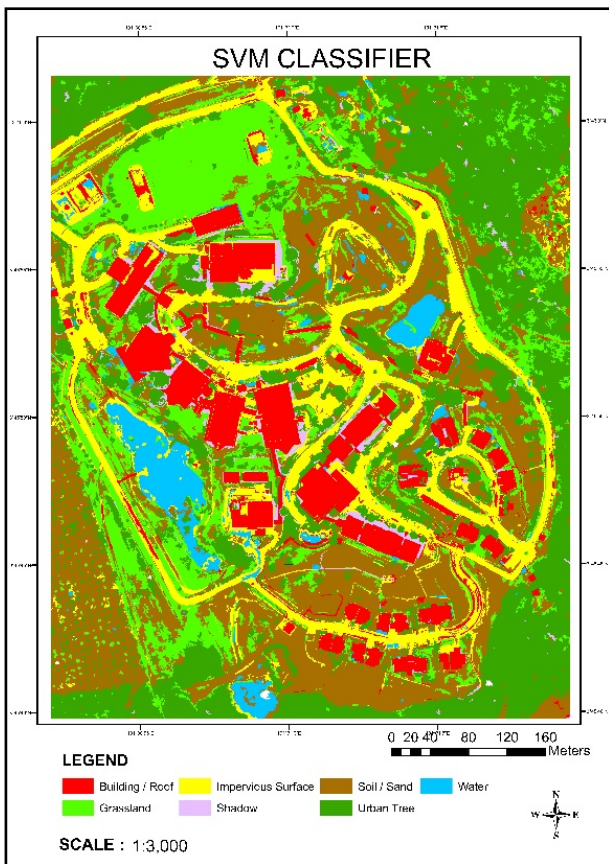


Figure 9b. SVM classification

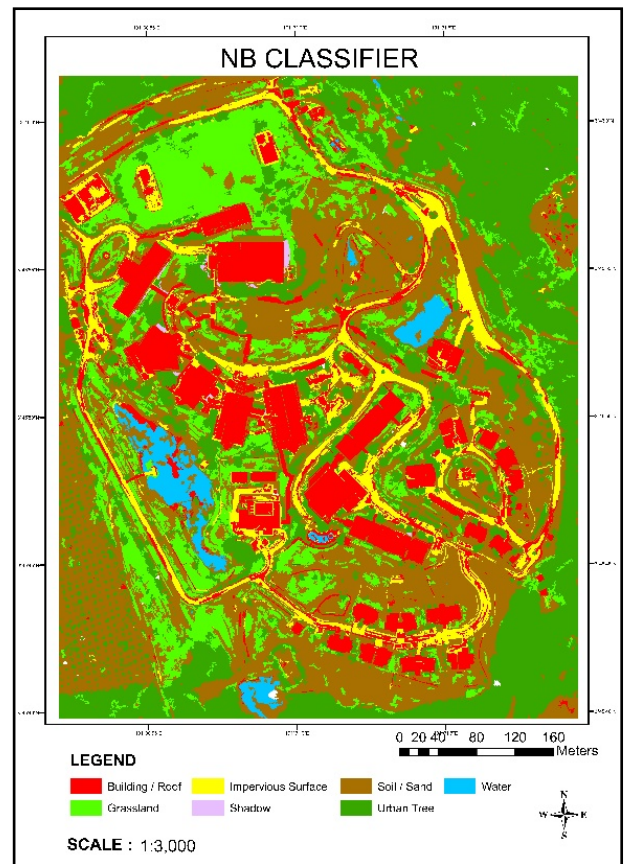


Figure 9d. NB classification

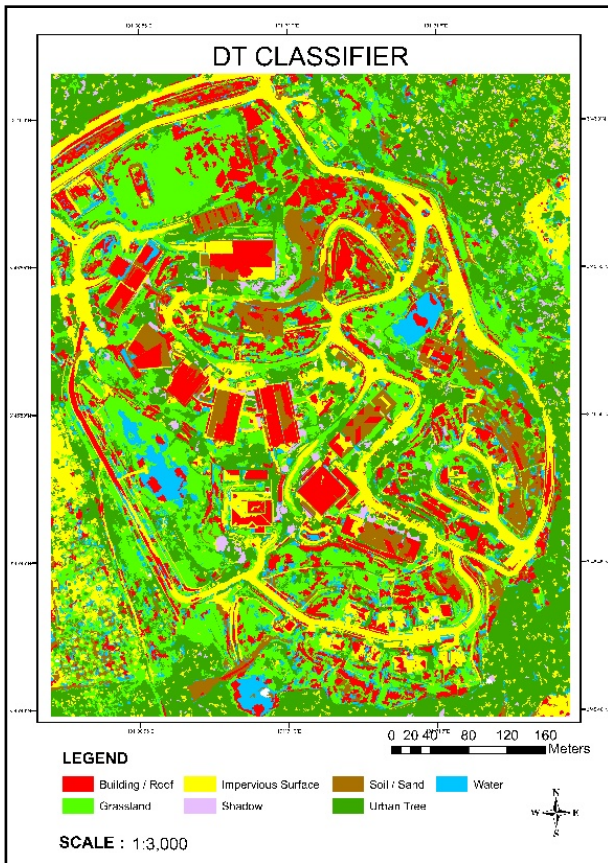


Figure 9e. DT classification

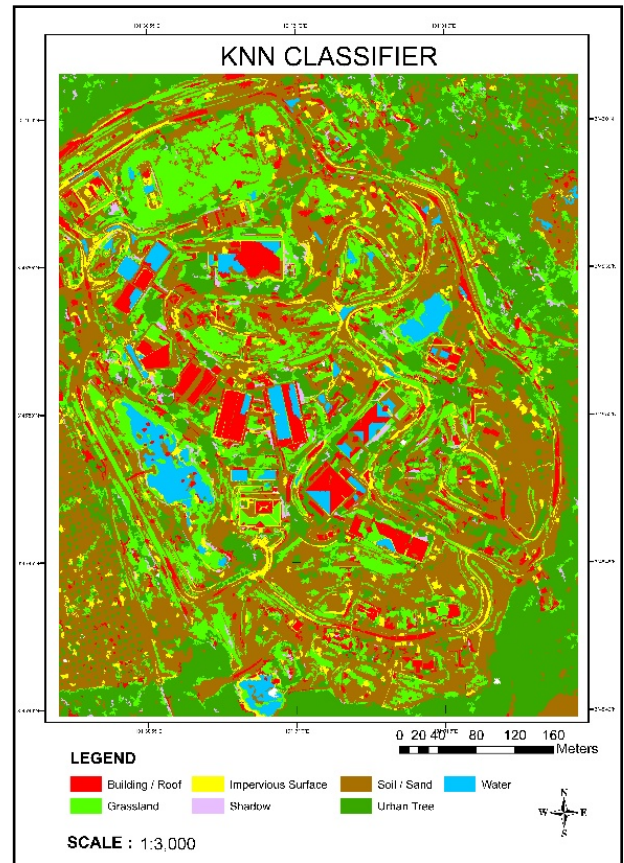


Figure 9f. KNN classification

Table 12. The best classification accuracy for each classifier

CLASSIFIER	SAMPLE DATA	PARAMETER	VALUE	OVERALL ACCURACY	KIA
NB	5	N/A	N/A	93.14	0.915
KNN	1	K NEIGHBORS	K=5	77.62	0.721
RF	2	MAXIMUM DEPTH	D=15	95.80	0.948
DT	1	MAXIMUM DEPTH	D=20	86.01	0.830
SVM	5	GAMMA, C	GAMMA = 0.001, C=100000	97.20	0.966

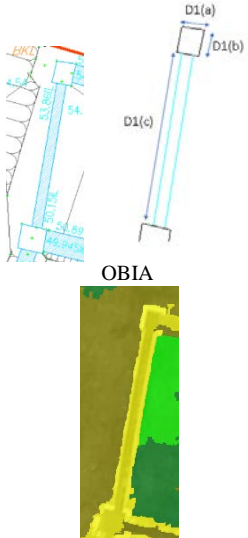
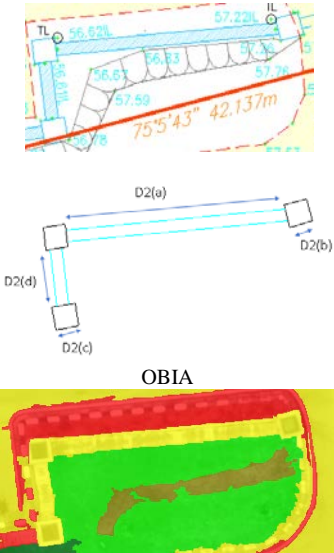
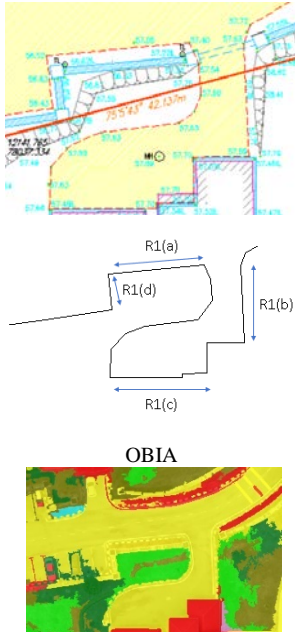
Table 13. Results of the McNemar test for each classifier

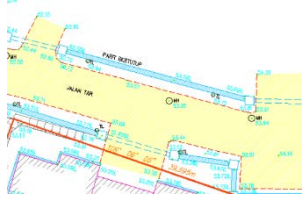
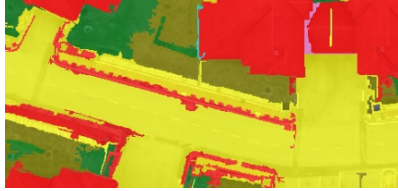
CLASSIFIER 1	CLASSIFIER 2	X ²	P value	SIGNIFICANT
SVM	RF	13.39535	0.0025	SIGNIFICANT
SVM	NB	9.63333	0.00191	SIGNIFICANT
SVM	DT	62.02532	0	SIGNIFICANT
SVM	KNN	51.8481	0	SIGNIFICANT
RF	NB	0.70588	0.4081	NOT SIGNIFICANT
RF	DT	31.64063	0	SIGNIFICANT
RF	KNN	27.16071	0	SIGNIFICANT
NB	DT	29.71429	0	SIGNIFICANT
NB	KNN	31.58209	0	SIGNIFICANT
DT	KNN	0.28409	0.59403	NOT SIGNIFICANT

Figures 9(a) to 9(f) present an orthomosaic of the study area and the result of the best classification for each classifier with the parameter indicated in Table 12. These findings present an important implication in the selection of appropriate classifiers. SVM outperformed the other classifiers and was the best classifier for land cover classification. The SVM classifier provided good overall classification for all sample data. NB can be an alternative

classifier when the training samples are sufficiently large. RF also shows the potential to obtain high accuracies as those of SVM with sufficient parameter setting.

The McNemar test indicated that the SVM classifier was highly significant compared with the other classifiers. Hence, SVM outperformed the other classifiers. The significant results of the McNemar test are presented in Table 13.

CLASSES	GROUND TRUTH (Acquired from Ground Truth Survey) & OBIA (Extraction from UAV data)	ERROR ASSESSMENT = Ground Truth (GT) - OBIA																					
Drainage 1	<p style="text-align: center;">CT</p>  <p style="text-align: center;">OBIA</p>	<table border="1" style="width: 100%; border-collapse: collapse;"> <thead> <tr> <th>CLASSES</th> <th>GT (m)</th> <th>OBIA (m)</th> <th>ERROR +/-</th> </tr> </thead> <tbody> <tr> <td rowspan="3">DRAINAGE, D1</td> <td>D1 (a)</td> <td>1.398</td> <td>1.526</td> <td>-0.128</td> </tr> <tr> <td>D1 (b)</td> <td>1.599</td> <td>1.507</td> <td>0.092</td> </tr> <tr> <td>D1 (c)</td> <td>10.462</td> <td>10.606</td> <td>-0.144</td> </tr> </tbody> </table>	CLASSES	GT (m)	OBIA (m)	ERROR +/-	DRAINAGE, D1	D1 (a)	1.398	1.526	-0.128	D1 (b)	1.599	1.507	0.092	D1 (c)	10.462	10.606	-0.144				
CLASSES	GT (m)	OBIA (m)	ERROR +/-																				
DRAINAGE, D1	D1 (a)	1.398	1.526	-0.128																			
	D1 (b)	1.599	1.507	0.092																			
	D1 (c)	10.462	10.606	-0.144																			
Drainage 2	<p style="text-align: center;">GT</p>  <p style="text-align: center;">OBIA</p>	<table border="1" style="width: 100%; border-collapse: collapse;"> <thead> <tr> <th>CLASSES</th> <th>GT (m)</th> <th>OBIA (m)</th> <th>ERROR +/-</th> </tr> </thead> <tbody> <tr> <td rowspan="4">DRAINAGE, D2</td> <td>D2 (a)</td> <td>12.865</td> <td>12.756</td> <td>0.109</td> </tr> <tr> <td>D2 (b)</td> <td>1.313</td> <td>1.517</td> <td>-0.204</td> </tr> <tr> <td>D2 (c)</td> <td>1.338</td> <td>1.255</td> <td>0.083</td> </tr> <tr> <td>D2 (d)</td> <td>3.308</td> <td>3.511</td> <td>-0.203</td> </tr> </tbody> </table>	CLASSES	GT (m)	OBIA (m)	ERROR +/-	DRAINAGE, D2	D2 (a)	12.865	12.756	0.109	D2 (b)	1.313	1.517	-0.204	D2 (c)	1.338	1.255	0.083	D2 (d)	3.308	3.511	-0.203
CLASSES	GT (m)	OBIA (m)	ERROR +/-																				
DRAINAGE, D2	D2 (a)	12.865	12.756	0.109																			
	D2 (b)	1.313	1.517	-0.204																			
	D2 (c)	1.338	1.255	0.083																			
	D2 (d)	3.308	3.511	-0.203																			
Road 1	<p style="text-align: center;">GT</p>  <p style="text-align: center;">OBIA</p>	<table border="1" style="width: 100%; border-collapse: collapse;"> <thead> <tr> <th>CLASSES</th> <th>GT (m)</th> <th>OBIA (m)</th> <th>ERROR +/-</th> </tr> </thead> <tbody> <tr> <td rowspan="4">ROAD, R1</td> <td>R1 (a)</td> <td>14.993</td> <td>14.880</td> <td>0.113</td> </tr> <tr> <td>R1 (b)</td> <td>12.425</td> <td>12.307</td> <td>0.118</td> </tr> <tr> <td>R1 (c)</td> <td>11.238</td> <td>11.114</td> <td>0.124</td> </tr> <tr> <td>R1 (d)</td> <td>5.533</td> <td>5.638</td> <td>-0.105</td> </tr> </tbody> </table>	CLASSES	GT (m)	OBIA (m)	ERROR +/-	ROAD, R1	R1 (a)	14.993	14.880	0.113	R1 (b)	12.425	12.307	0.118	R1 (c)	11.238	11.114	0.124	R1 (d)	5.533	5.638	-0.105
CLASSES	GT (m)	OBIA (m)	ERROR +/-																				
ROAD, R1	R1 (a)	14.993	14.880	0.113																			
	R1 (b)	12.425	12.307	0.118																			
	R1 (c)	11.238	11.114	0.124																			
	R1 (d)	5.533	5.638	-0.105																			

CLASSES	GROUND TRUTH (Acquired from Ground Truth Survey) & OBIA (Extraction from UAV data)	ERROR ASSESSMENT = Ground Truth (GT) - OBIA																					
CLASSES	GROUND TRUTH (Acquired from Ground Truth Survey) & OBIA (Extraction from UAV data)	ERROR ASSESSMENT = Ground Truth (GT) - OBIA																					
Road 2	<p>GT</p>  <p>R2(d) R2(a)</p> <p>R2(c) R2(b)</p> <p>OBIA</p> 	<table border="1"> <thead> <tr> <th>CLASSES</th> <th>GT (m)</th> <th>OBIA (m)</th> <th>ERROR +/-</th> </tr> </thead> <tbody> <tr> <td rowspan="4">ROAD, R2</td> <td>R2 (a)</td> <td>5.597</td> <td>5.482</td> <td>0.115</td> </tr> <tr> <td>R2 (b)</td> <td>10.501</td> <td>10.59</td> <td>-0.089</td> </tr> <tr> <td>R2 (c)</td> <td>5.595</td> <td>5.711</td> <td>-0.116</td> </tr> <tr> <td>R2 (d)</td> <td>29.234</td> <td>29.351</td> <td>-0.117</td> </tr> </tbody> </table>	CLASSES	GT (m)	OBIA (m)	ERROR +/-	ROAD, R2	R2 (a)	5.597	5.482	0.115	R2 (b)	10.501	10.59	-0.089	R2 (c)	5.595	5.711	-0.116	R2 (d)	29.234	29.351	-0.117
CLASSES	GT (m)	OBIA (m)	ERROR +/-																				
ROAD, R2	R2 (a)	5.597	5.482	0.115																			
	R2 (b)	10.501	10.59	-0.089																			
	R2 (c)	5.595	5.711	-0.116																			
	R2 (d)	29.234	29.351	-0.117																			

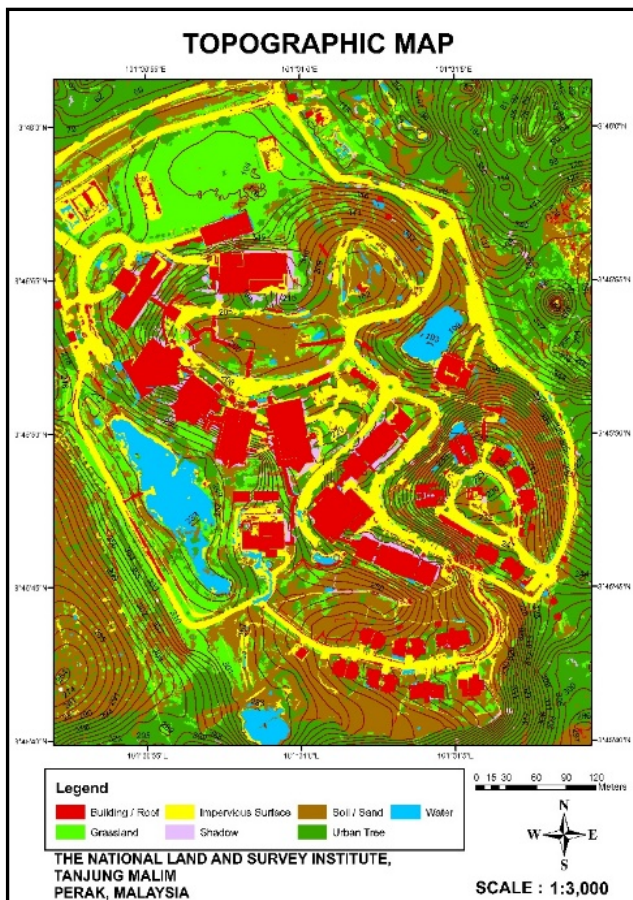


Figure 10. Final topographic map based on the best accuracy of the SVM classifier

4. Conclusion

We have evaluated and compared the performance of five machine learning classifiers in classifying high-resolution images by implementing an OBIA procedure. The SVM classifier obtained the highest results among all classifiers. The classification was affected by the accuracy of the tuning parameters for each classifier when different sizes of training and testing samples were used.

The extraction of as-built information was examined through a geometrical assessment with the output of the data extraction. The tolerance of as-built information (building, drainage and road) through the ground truth data using survey equipment (total station) with UAV OBIA data obtained an error of less than 1 metre. The combination of UAV and OBIA can provide a rapid and efficient approach for map updating, especially in rapidly changing urban areas. This technique can potentially replace current procedures that utilise piloted aircraft and high-resolution satellite data (more expensive and time consuming). Hence, the results of this study provide an additional insight into the use of OBIA for UAV optical imagery information extraction.

Acknowledgements

The authors would like to thank the National Land and Survey Institute for providing and sharing UAV data to realise this research. Gratitude is also extended to the staff of Photogrammetry Section, Division of Topography Mapping, Department of Survey and Mapping Malaysia

(JUPEM) for their contributions, ideas, comments and criticisms on the current issues related to the scope of the study. UPM is also acknowledged for the provision of financial support via the GRF scheme. Comment from the anonymous reviewers are highly appreciated.

References

- [1] Ahmad, A., Hashim, K. A., & Samad, A. M. (2010). Aerial Mapping using High Resolution Digital Camera and Unmanned Aerial Vehicle for Geographical Information System. *2010 6th International Colloquium on Signal Processing & Its Applications (CSPA)*, 201-206.
- [2] Hardin, P. J., & Hardin, T. J. (2010). Small-scale remotely piloted vehicles in environmental research. *Geography Compass*, 4(9), 1297-1311.
- [3] Laliberte, A. S., & Rango, A. (2009). Texture and Scale in Object-Based Analysis of Subdecimeter Resolution Unmanned Aerial Vehicle (UAV) Imagery. *IEEE Transactions on Geoscience and Remote Sensing*, 47(3), 761-770.
- [4] Nex, F., & Remondino, F. (2014). UAV for 3D mapping applications: A review. *Applied Geomatics*, 6(1), 1-15.
- [5] Ahmad, A. (2016). *The Direction of UAV Technology in Malaysia & The Principle of Photogrammetry for UAV Mapping*. PowerPoint presentation at the courses of UAV Technology and Image Processing, The National and Survey Institute (INSTUN), Perak, Malaysia.
- [6] Mohammadi, M., Hahn, M., & J, E. (2011). Road Classification and Condition Investigation Using Hyperspectral Imagery. In *Applied Geoinformatics for Society and Environment*. Jomo Kenyatta University of Agriculture and Technology Stuttgart University of Applied Sciences.
- [7] Crommelinck, S., Bennett, R., Gerke, M., Nex, F., Yang, M. Y., & Vosselman, G. (2016). Review of automatic feature extraction from high-resolution optical sensor data for UAV-based cadastral mapping. *Remote Sensing*, 8(689).
- [8] Jazayeri, I., Rajabifard, A., & Kalantari, M. (2014). A geometric and semantic evaluation of 3D data sourcing methods for land and property information. *Land Use Policy*, 36, 219-230.
- [9] Blaschke, T., Lang, S., Lorp, E., Strobl, J., & Zeil, P. (2000). Object-Oriented Image Processing in an Integrated GIS / Remote Sensing Environment and Perspectives for Environmental Applications. *Environmental Information for Planning, Politics and the Public*, (1995), 555-570.
- [10] Gibril, M. B. A., Shafiq, H. Z. M., & Hamedianfar, A. (2017). New semi-automated mapping of asbestos cement roofs using rule-based object-based image analysis and Taguchi optimization technique from WorldView-2 images. *International Journal of Remote Sensing*, 38(2), 467-491.
- [11] Ma, L., Li, M., Ma, X., Cheng, L., Du, P., & Liu, Y. (2017). A review of supervised object-based land-cover image classification. *ISPRS Journal of Photogrammetry and Remote Sensing*, 130, 277-293.
- [12] Tzotsos, A., Karantzalos, K., & Argialas, D. (2010). Object-based image analysis through nonlinear scale-space filtering. *ISPRS Journal of Photogrammetry and Remote Sensing*, 66(1), 2-16.
- [13] Rao, R. S., Kumar, C. G., Prakasham, R. S., & Hobbs, P. J. (2008). The Taguchi methodology as a statistical tool for biotechnological applications: A critical appraisal. *Biotechnology Journal*, 3(4), 510-523.
- [14] Idrees, M. O., & Pradhan, B. (2016). Hybrid Taguchi-Objective Function optimization approach for automatic cave bird detection from terrestrial laser scanning intensity image. *International Journal of Speleology*, 45(3), 289-301.
- [15] Moosavi, V., Talebi, A., & Shirmohammadi, B. (2013). Producing a landslide inventory map using pixel-based and object-oriented approaches optimized by Taguchi method Vahid. *Geomorphology*.
- [16] Sameen, M. I., & Pradhan, B. (2017). A Two-Stage Optimization Strategy for Fuzzy Object-Based Analysis Using Airborne LiDAR and High-Resolution Orthophotos for Urban Road Extraction, 2017.
- [17] Majeed, Z. A., Saip, S. N., & Ng, E. G. (2017). Towards augmented topographic map: Integration of digital photograph captured from MAV and UAV platform. In *FIG Working Week 2017 Presentation Paper* (pp. 1-15).
- [18] Ma, L., Cheng, L., Li, M., Liu, Y., & Ma, X. (2015). Training set size, scale, and features in Geographic Object-Based Image Analysis of very high resolution unmanned aerial vehicle imagery. *ISPRS Journal of Photogrammetry and Remote Sensing*, 102, 14-27.
- [19] Qian, Y., Zhou, W., Yan, J., Li, W., & Han, L. (2015). Comparing Machine Learning Classifiers for Object-Based Land Cover Classification Using Very High Resolution Imagery. *Remote Sensing*, 7, 153-168.
- [20] Sharma, J. B., & Hulsey, D. (2014). Integrating the UAS in Undergraduate Teaching and Research - Opportunity and Challenges at The University of Georgia. In *The International Archives of the Photogrammetry, Remote Sensing and Spatial Information Sciences. ISPRS Technical Commission I Symposium* (Vol. XL, pp. 17-20).
- [21] Grigillo, D., & Kanjir, U. (2012). Urban object extraction from digital surface model and digital aerial images. In *ISPRS Annals of the Photogrammetry, Remote Sensing and Spatial Information Sciences* (Vol. 1-3, pp. 215-220).
- [22] Murcko, J. (2017). *Object-based classification for estimation of built-up density within urban environment*.
- [23] Suzuki, K., Liu, W., Estrada, M., & Yamazaki, F. (2013). Object-based building extraction in Tacna, Peru using worldview-2 images. In *Proceedings of ACRS 2013* (pp. 1159-1166).
- [24] Tomljenovic, I., Tiede, D., & Blaschke, T. (2016). A building extraction approach for Airborne Laser Scanner data utilizing the Object Based Image Analysis paradigm. *International Journal of Applied Earth Observations and Geoinformation*, 52, 137-148.
- [25] Kavzoglu, T., & Yildiz, M. (2014). Parameter-Based Performance Analysis of Object-Based Image Analysis Using Aerial and Quickbird-2 Images. *ISPRS Annals of the Photogrammetry, Remote Sensing and Spatial Information Sciences, Volume II-7, 2014, II(October)*, 31-37.
- [26] Baatz, M., & Schäpe, A. (2000). Multiresolution segmentation: An optimization approach for high quality multi-scale image segmentation. *Proceedings of Angewandte Geographische Informationsverarbeitung XII*, 12-23.
- [27] Martha, T. R., Kerle, N., Van Westen, C. J., Jetten, V., & Kumar, K. V. (2011). Segment optimization and data-driven thresholding for knowledge-based landslide detection by object-based image analysis. *IEEE Transactions on Geoscience and Remote Sensing*, 49(12 PART 1), 4928-4943.
- [28] Li, C., & Shao, G. (2012). Object-oriented classification of land use / cover using digital aerial orthophotography. *International Journal of Remote Sensing*, 33, 922-938.
- [29] Lowe, S. H., & Guo, X. (2011). Detecting an Optimal Scale Parameter in Object-Oriented Classification. *IEEE Journal of Selected Topics in Applied Earth Observations and Remote Sensing*, 4(4), 890-895.
- [30] Pu, R., Landry, S., & Yu, Q. (2011). Object-based urban detailed land cover classification with high spatial resolution IKONOS imagery, 32(12), 3285-3308.
- [31] Chou, C.-S., Ho, C.-Y., & Huang, C.-I. (2009). The optimum conditions for comminution of magnetic particles driven by a rotating magnetic field using the Taguchi method. *Advanced Powder Technology*, 20(1), 55-61.
- [32] Aggarwal, A., Singh, H., Kumar, P., & Singh, M. (2008). Optimizing power consumption for CNC turned parts using response surface methodology and Taguchi's technique-A comparative analysis. *Journal of Materials Processing Technology*, 200(1-3), 373-384.
- [33] Pradhan, B., Jebur, M. N., Shafi, H. Z. M., & Tehrani, M. S. (2015). Data Fusion Technique Using Wavelet Transform and Taguchi Methods for Automatic Landslide Detection From Airborne Laser Scanning Data and QuickBird Satellite Imagery. *IEEE Transactions on Geoscience and Remote Sensing*, 1-13.
- [34] Espindola, G. M., Camara, G., Reis, I. A., Bins, L. S., & Monteiro, A. M. (2006). Parameter selection for region-growing image segmentation algorithms using spatial autocorrelation. *International Journal of Remote Sensing*, 27(14), 3035-3040.

- [35] Gao, Y., Kerle, N., Mas, J. F., Navarrete, A., & Niemeyer, I. (2007). Optimized Image Segmentation and Its Effect on Classification Accuracy. *5th International Symposium - Spatial Data Quality*, 4p. Retrieved from http://www.itc.nl/ISSDQ2007/proceedings/postersession/gao_kerleet_al.pdf.
- [36] Fotheringham, A. S., Brunson, C., & Charlton, M. (2000). *Quantitative Geography: Perspectives on Spatial Data Analysis*. Cleveland State University.
- [37] Wieland, M., & Pittore, M. (2014). Performance evaluation of machine learning algorithms for urban pattern recognition from multi-spectral satellite images. *Remote Sensing*, 6(4), 2912-2939.
- [38] Trimble. (2014). *eCognition © Developer*. User Guide.
- [39] Nichol, J., & Wong, M. S. (2008). Habitat Mapping in Rugged Terrain Using Multispectral Ikonos Images. *Photogrammetric Engineering & Remote Sensing*, 74(11), 1325-1334.
- [40] Foody, G. M. (2002). Status of land cover classification accuracy assessment. *Remote Sensing of Environment*, 80(1), 185-201.
- [41] Congalton, R. G., & Green, K. (1993). A Practical Look at the Sources of Confusion in Error Matrix Generation. *American Society for Photogrammetry and Remote Sensing*, 59(5), 641-644.
- [42] Hamedianfar, A., Shafri, H. Z. M., Mansor, S., & Ahmad, N. (2014). Improving detailed rule-based feature extraction of urban areas from WorldView-2 image and lidar data. *International Journal of Remote Sensing*, 35(5), 1876-1899.
- [43] Foody, G. M. (2004). Thematic map comparison: evaluating the statistical significance of differences in classification accuracy. *Photogrammetric Engineering & Remote Sensing*, 70(5), 627-633.
- [44] Leeuw, J. D., Jia, H., Yang, L., Schmidt, K., & Skidmore, A. K. (2006). Comparing accuracy assessment to infer superiority of image classification methods. *International Journal of Remote Sensing*, 27(1), 223-232.
- [45] Goebel, K., & Saha, B. (2015). *Handbook of Unmanned Aerial Vehicles*. Springer Reference. Springer Dordrecht Heidelberg New York London.
- [46] Husran, Z. (2016, November 8). *The use of UAV Technology in Planning and Security Monitoring*. PowerPoint presentation at the courses of UAV Technology and Image Processing, The National and Survey Institute (INSTUN), Perak, Malaysia.
- [47] International Civil Aviation Organization (ICAO) (Ed.). (2011). *Unmanned Aircraft Systems (UAS)*. University Street, Montréal, Quebec, Canada.
- [48] JUPEM (2010). JUPEM: A pictorial journey 1885-2010 (Commemorating the 125th Anniversary). Kuala Lumpur, Malaysia.
- [49] Rabab, M.Z.M (2012). *UAV capabilities for the purpose of Data Acquisition for geospatial defence data*. Berita Ukur July – December 2012. Malaysia.
- [50] Wang, T. Y., & Huang, C. Y. (2007). Improving forecasting performance by employing the Taguchi method. *European Journal of Operational Research*, 176(2), 1052-1065.